Biosensors and Bioelectronics 167 (2020) 112498

Contents lists available at ScienceDirect

Biosensors and Bioelectronics

journal homepage: http://www.elsevier.com/locate/bios

Biolayer interferometry-SELEX for Shiga toxin antigenic-peptide aptamers & detection via chitosan-WSe_2 aptasensor

Harmanjit Kaur [2], Munish Shorie [2], Priyanka Sabherwal [*,1]

Institute of Nano Science & Technology, Mohali, 160062, India

ARTICLE INFO

Keywords:
Biolayer interferometry (BLI)
SELEX
In-vitro diagnostics
Protein biosensor
Shiga toxin
Tungsten diselenide

ABSTRACT

We report biolayer interferometry based *in-vitro* selection technique (BLI-SELEX) for fishing out specific aptamers against *E. coli* Shiga toxin subtypes *viz.,* stx1 & stx2 via epitopic peptides. BLI-SELEX is a one-step technique for rapidly generating aptamers against protein biomarkers in a microtiter plate format, obliterating the need for multiple enrichment rounds to harvest high-affinity aptamers as in conventional SELEX. Two unique aptamers selected against stx1 & stx2 with picomolar K_d (~47 pM & ~29 pM, respectively) were successfully used to fabricate voltammetric diagnostic assay via immobilization onto chitosan exfoliated 2D tungsten diselenide (WSe_2) nanosheet platform. These aptamers modified nanosensors showed high sensitivity of ~ 5.0 μA ng^{-1} mL, a dynamic response range from 50 pg mL^{-1} to 100 ng mL^{-1}, with a detection limit of 44.5 pg mL^{-1} & 41.3 pg mL^{-1} for stx subtypes, respectively and showed low cross-reactivity in spiked urine, serum and milk samples. The synergistic effect of selective aptamers & high sensitivity imparted by 2D transition metal dichalcogenide (TMD) highlights the superior potential of a fabricated nanosensor for bacterial toxin detection.

1. Introduction

Since the inception of, systematic evolution of ligands by exponential enrichment (SELEX), 'aptamers' with the ability to bind specific ligands with high affinities have been purported as next-gen antibody mimics (Panigaj et al., 2019; Tuerk and Gold, 1990). These single-stranded nucleic acid molecules screened *in-vitro* via iterated alternate rounds of selection & amplification, harbor pico-nanomolar affinities & high target selectivity (Goto et al., 2017; Negahdary, 2020). These strikingly appreciable recognition moieties arise out of a milieu of random & unique sequences, binding to their target of interest via non-covalent interactions (Dupont et al., 2015). As opposed to conventional antibodies, chemically synthesized aptamers negate the need of animal models, showing no batch variations and can also be screened for a wide range of infectious or non-immunogenic entities, thwarting the position of antibodies as lead receptor type in biosensors (Pehlivan et al., 2019; Sharifi et al., 2020; Villalonga et al., 2020). Over the last three decades, although numerous labs have reported SELEX variants, a majority of these are modulations of traditional multiple iteration technique, thus rendering them relatively slow & cumbersome (Wang et al., 2019). Especially in urgent global scenarios, these are impractical beyond basic research in lab settings (Kelly-Cirino et al., 2019).

Shiga toxin-producing *Escherichia coli* (STEC), a major source of food poisoning associated with 2.5 million cases annually, has a low infectious dose of 100 cells enough for disease manifestation (Kirk et al., 2015). As the sequalae hemolytic-uremic syndrome is persistent in 5–15% cases, which entails hemolytic anemia, thrombocytopenia & nephron damage. This damage is a direct result of hemolytic & rRNA-glycosidase activity of Shiga-like toxins (stx). These are proteinous toxins, which bind via B_5 subunit to specific glycolipids (Gb3/Gb4) abundantly present on microvascular cells of the kidney, colon, and central nervous system (Kavaliauskiene et al., 2017). Though similar in action, its subtypes (stx1 & stx2) are non-homologous, sharing only ~56% sequence identity amongst themselves. It has been reported that stx2 (LD_{50} of 50 ng kg^{-1}) is 100 times more lethal than stx1 (Rahman et al., 2018). Moreover, lack of vaccines, neutralizing drugs & unjustified antibiotic therapy further aggravates the condition leading to the systemic release of toxins. Therefore, specific identification in clinical samples is essential. The current detection techniques revolve around culture identification or PCR based screening using *stx1/stx2* specific

* Corresponding author.
E-mail addresses: priyanka.sabherwal@nano.mu.ac.in, psnanobiotech@gmail.com (P. Sabherwal).
[1] Current address. National Centre for Nanoscience & Nanotechnology, University of Mumbai, Mumbai-400098, India.
[2] These authors contributed equally.

https://doi.org/10.1016/j.bios.2020.112498
Received 26 May 2020; Received in revised form 30 July 2020; Accepted 3 August 2020
Available online 6 August 2020

primers requiring extensive sampling, expensive machinery & skilled personnel for analyses (Vallières et al., 2013). So far, only a few studies of polyclonal antibodies, a camelid antibody, and two low-affinity aptamers have been reported (Challa et al., 2014; He et al., 2013; Mejías et al., 2016). Thus, a niche is promised for aptamers as recognition moiety for stx subtypes. Correspondingly, conventionally employed diagnostics platforms are antibody-based, which are costly, suspectable to denaturation, and show cross-talk amongst subtypes. In search of minimal cross-talk receptors, it is also essential that the highest affinity receptors against prominently distinct surface epitopes result in maximum binding (Correia et al., 2014). In accordance, different surface-exposed epitopes present on the toxin subunit have been explored one-by-one for aptamer-based receptor generation in our study. This methodology aids in decoding, the leading peptide epitope for bio-receptor interaction and as well as, assists the subsequent selection of best aptamer to the toxin.

Aptamers conferred with high selectivity & binding affinities have been lately exploited for diagnostic & therapeutic applications (Kaur et al., 2020; Kudłak and Wieczerzak, 2020). Needless to say, the integration of specific aptamers with 2D nanomaterials has opened avenues for the development of high sensitivity low-cost electrochemical diagnostic platforms (Li et al., 2019; Shorie et al., 2018). Recent advances in TMDs are focused on tungsten dichalcogenide due to their unique physical & chemical properties particularly, tunable direct bandgap corresponding to atomic layers (Rahmanian et al., 2018; Shi et al., 2020; Shorie et al., 2018). Exploiting the semi-conductive nature of WSe_2, we employed a green exfoliating method using an aqueous suspension of chitosan for simultaneous exfoliation & functionalization of layered WSe_2 and subsequent immobilization of our selected aptamers for sensing application. For the electrochemical studies, square-wave voltammetry (SWV) was used for analytical measurements, which is a rapid & reliable electrochemical technique capable of generating sensing results in a short time (Chen and Shah, 2013; Ikebukuro et al., 2004; Meirinho et al., 2016). This voltammetric detection method is widely used for sensitive detection of biomolecules and allows quantitative sensing of Shiga toxin subtypes in a simplified, cost-effective chip format. This platform gives an edge over immunoassays as label-free technology with high sensitivity to the presence of target antigens in real samples and, thus, is explored in this study as the detection technique. Hence, a pragmatic approach towards the development of a robust alternative, biolayer interferometry (BLI) based SELEX has been successfully achieved, enabling rapid selection of aptamers against protein biomarkers in a single microplate format eliminating the need of enrichment iterations and concomitantly allowing real-time monitoring of SELEX progression & binding affinity. Using this methodology, we targeted Shiga toxin subtypes for the selection of novel high-affinity aptamers and demonstrated its detection over voltammetric sensors.

As illustrated in Fig. 1, our current study revolves around two major aspects of an efficient biosensor, namely; (a) facile selection of novel aptamers against protein toxins, herein exploiting antigenically distinct peptide epitopes of stx1 & stx2 using a single microplate format screening and monitoring via biolayer interferometry (BLI) platform followed by (b) voltammetric sensing of the toxins using individual-specific aptamer functionalized onto Chito-WSe_2 electrochemical platforms.

2. Experimental

2.1. Materials

NaCl, KCl, Na_2HPO_4, KH_2PO_4, $MgCl_2$, potassium ferrocyanide ($K_4[Fe(CN)_6]\cdot 3H_2O$), potassium ferricyanide ($K_3[Fe(CN)_6]$), anhydrous acetic acid, EDC, sulfo-NHS, MES sodium salt, and ethanolamine were purchased from Merck (India). Tungsten (IV) Selenide 99.8% from Alfa Aesar (India), chitosan (Low MW) extra pure was purchased from SRL (India), and fetal bovine serum (FBS) from Gibco (India). Purified &

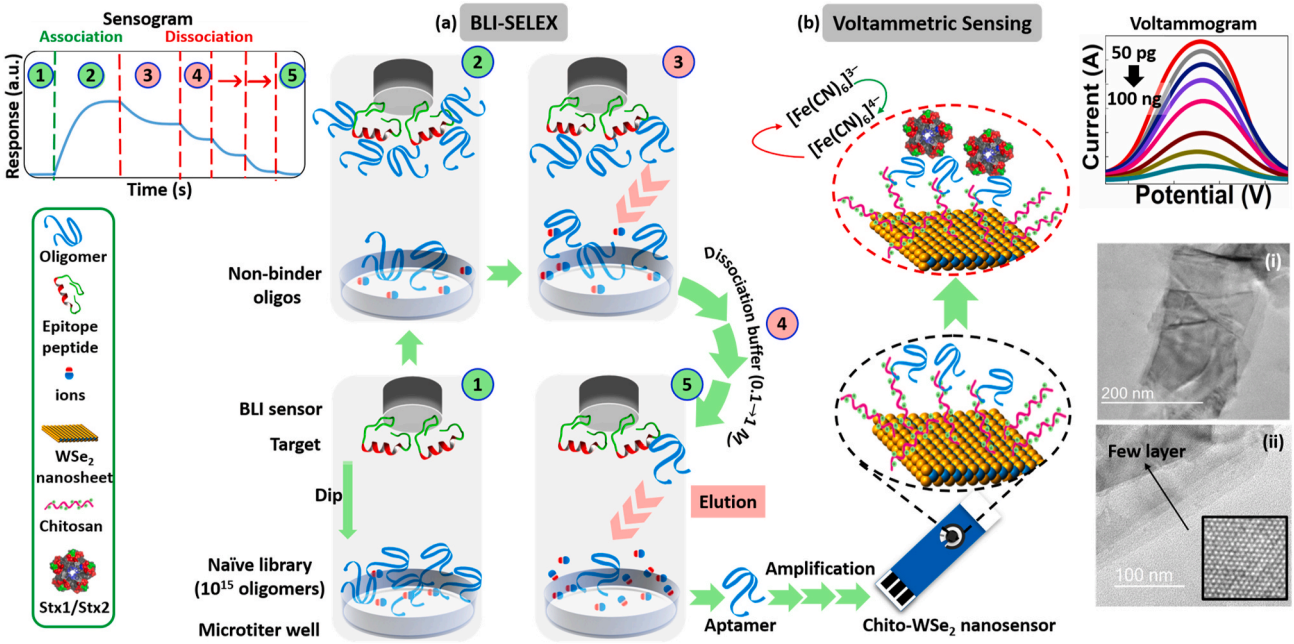

Fig. 1. Schematic Illustration. An illustration of (a) step-by-step BLI based SELEX showing (1) selected epitope peptide of Stx (*bait*) bound on BLI sensor being dipped into microtiter well having a pool of random oligomers (naïve library) (2) wherein, a few interact & associate with the target, while the non-binders are retained in the bottom well itself. These fished-out binder oligomers (3) dissociate from the target in different wells having buffers with sequentially increasing ionic concentrations (0.1–1M). (4) The oligomers with affinity in ascending order to target are shed-out in respective dissociation buffer wells and (5) eluted out for quantification, amplification & characterization. A BLI sensogram showing the characteristic real-time kinetics is illustrated alongside. These well 'aptamers' were used for functionalization of (b) Chito-WSe_2 modified electrochemical nanosensor for the detection of stx1 & stx2, individually. The voltammetric sensing (using 1 mM $[Fe(CN)6]^{3-/4-}$ redox probe) shows a linear current decrease with the subsequent addition of 50 pg–100 ng of specific toxin subtype. Also, TEM images of Chito-WSe_2 showing (i) layered nanosheet morphology, (ii) distinct few layers & (*inset*) high-resolution image showing hexagonal lattice structure.

characterized custom peptides were synthesized from Xcelris Genomics (India), purified *E. coli stx*1b and stx2b were purchased from MyBioSource, Inc (USA), purified single-stranded oligonucleotide naive library of an internal random region of 45 nucleotides (5′-ATCCAGAGTGACGCAGCA-(N45)-TGGACACGGTGGCTTAGT-3′) flanked by 18 nucleotides primer binding sites at 5′ and 3′ ends along with forward primer (5′-ATCCAGAGTGACGCAGCA-3′) and biotinylated reverse primer (5′-biotin-ACTAAGCCACCGTGTCCA-3′) were synthesized from Sigma-Aldrich (India). All the aqueous solutions were prepared using nuclease-free water, MP biomedicals (India).

2.2. Peptide epitope screening

The protein sequences of stx1b and stx2b (accession no. NP_311000.1, NP_309233.1) retrieved from GenPept (NCBI database) were used to screen antigenic sites (Supporting Information ST1). These epitopes were processed using an online immunogenicity tool (http://imed.med.ucm.es/Tools/antigenic.pl), which predicts antigenic segments from within a protein sequence based on the propensity of amino acid residues in experimentally known epitopes. The surface accessibility of the selected antigenic sites was determined using the NetsurfP server (Klausen et al., 2019). The tertiary structure of the energy minimized epitopes were analyzed using the PEPstr tool & Yasara view (Kaur et al., 2007; Krieger et al., 2002). The selected antigenic peptides of the two toxin subtypes were custom synthesized and utilized in studies without further modification for aptamer selection.

2.3. Biolayer interferometry-based SELEX

The BLI-SELEX based aptamer selection was carried out on the BLI instrument, Octet® Red96 system (FortéBio), using a 96-well plate in kinetics mode (Supporting Information ST2). Before the loading of the target peptide onto the amine-reactive 2nd generation (AR2G) sensors, the sensors were hydrated for 15 min in biosensor tray inside the Octet instrument set at 37 °C for optimum kinetics. The next steps were: *(i) Target immobilization:* The AR2G sensors were activated using freshly prepared 20 mM EDC:10 mM NHS that generate reactive NHS esters. The peptides (40 μg mL^{-1}) prepared in 10 mM MES buffer (pH 5.5) were allowed to couple with NHS esters resulting in surface immobilization. The unreacted free groups were quenched by dipping in 0.5M ethanolamine (pH 8) and the baseline set. Table S1 details the loading parameters used in the study. *(ii) Selection:* The conditioned naïve library (1 μM) diluted in binding buffer (>10^{14} oligomers) was exposed to an AR2G sensor loaded with the target peptide. The binders that associate with target were fished out of the random pool of oligomers & sequentially dissociated into different microtiter wells containing dissociation buffer of increasing ionic strength in accordance to binding affinity (0.1–1M). Table S2 details the loading parameters used in the study, and schematically explained in Fig. S1. To further enrich the binder population (given copy number of aptamers may be low), the process was iterated five times. The elutes were collected, quantified, purified & amplified as per the authors' previous works (Kaur et al., 2017). Similarly, this process was carried out for all the epitope peptides of the two toxins, result datasets normalized against reference sensor, and globally fitted using a 1:1 binding model using FortéBio Data analysis 8.

2.4. Aptamer-antigen interaction studies

The positive aptamer pools selected against each epitope peptide were analyzed to confirm their affinity against peptides using BLI. For these aptamer-epitope interaction studies, the individual peptide-loaded sensors were dipped into the selected pool solution (2.5 μg), and the association/dissociation kinetics for 200 s was observed. The pools with the best binding affinity to each target epitope were chosen, and further, their interaction with the toxin was also confirmed. BLI kinetics at various concentrations of the individual champion aptamers ranging from 0, 25, 50–100 nM were carried out, and the average K_d value determined. The champion aptamer for each of the toxin subtypes was further scrutinized to corroborate the binding results using plate-binding assays (Supporting Information ST3). The selected aptamers with the highest affinity for the toxin subtypes were cloned & sequenced as per previous works (Kumar et al., 2016). The obtained sequences were characterized by structure modeling & docking studies using various bioinformatic tools (Supporting Information ST4). These fully characterized aptamers were used to detect stx1 & stx2 using electrochemical platforms.

2.5. Synthesis & characterization of Chito-WSe_2 nanosensor

The exfoliation of layered WSe_2 flakes was carried out via a modified liquid exfoliation protocol (Uysal Unalan et al., 2015). The concentration of exfoliant chitosan was optimized, and finally, 2.5 mg mL^{-1} was dissolved in 2 mL aqueous acetic acid (0.5% v/v, pH 6.5), along with bulk WSe_2 powder (1 mg mL^{-1}) and thoroughly vortexed. This dispersion was then probe sonicated for 30 min (30% amplitude, 5 s pulsated on/off cycles). The unexfoliated bulk was removed by centrifugation (1000×*g*, 10 min) and the supernatant siphoned out. Further, extensive rinsing of dispersions with distilled water was carried out to remove excess unused chitosan. The exfoliated nanomaterial was vacuum dried & re-dispersed (1 mg mL^{-1}). These chitosan exfoliated & functionalized WSe_2 nanosheets were characterized using various spectrophotometric, microscopic & electrochemical tools (Supporting Information ST5) and finally used for modification of electrochemical sensors as shown in Fig. S2.

2.6. Toxin detection: Aptamer mediated voltammetric assay

Chito-WSe_2 (1 mg mL^{-1}) was used to modify the working electrode of the screen-printed electrode (SPE). The concentration was optimized by a stepwise increase in the volume of drop-casted nanomaterial & subsequent drying at 40 °C. For bio-receptor functionalization, the selected aptamers (2.5 μg) were diluted in binding buffer (pH 7), drop-casted on the modified sensor surface, and incubated overnight at 4 °C. The sensor surface was rinsed with distilled water to remove any un-immobilized molecules and stored at 4 °C when not in use. Cyclic voltammetry (CV), electrochemical impedance spectroscopy (EIS), and square wave voltammetry (SWV) techniques were employed for sensor characterization using CHI760E electrochemical workstation (Supplementary Information ST6). The sensing bioassay was carried out using SWV, wherein varying amounts of stx1 & stx2 (0.01–1000 ng mL^{-1}) were subjected for 10 min each, followed by washing & voltammetric scanning. The voltammograms were recorded, and the current maxima vs. toxin concentration plotted to analyze the range of detection & limit of detection (LOD). The cross-reactivity of the individual Apta-nanosensors was investigated with bovine serum albumin (BSA), purified *E. coli* O157:H7 endotoxin, and the subtypes stx1 for stx2 sensor & vice-versa. Also, the performance of the aptasensor was demonstrated by spiking stx1 & stx2 in pre-processed real samples with complex matrices viz., cow milk, FBS & human urine (Supplementary Information ST7).

3. Results & discussion

3.1. Antigenic epitope screening of E. coli toxin

A biomolecule like protein forms various folded conformations based on its primary sequence along with the interplay of inter & intramolecular interactions, which provide three-dimensional stability. These collectively form various structures, where each different motif or subunit may have many different surface-exposed antigen determinants. Therefore, immune responses are directed against the various exposed antigenic sites of the protein, with antibodies binding to different regions with varied preferences or binding efficiency. It is well known that bio-receptors are generated against particular stretches known as

antigen determinants or epitopes rather than the whole protein. Thus, exploiting this notion, the toxin subtypes were screened for surface-exposed epitopes lying in non-homologous regions to impart selectivity to the receptors that would be generated against them. In supporting information ST8, Fig. S3 denotes three distinct epitopes for each stx subtypes with >20% surface accessibility, with motifs rich in α-helix & β-turn, which are reported to be present in the recognition domains of known proteins (Kozlova et al., 2018). The localization of predicted epitopes on the exposed surface of toxins in Fig. S4 confirmed the same. Thus, the aptamer generation was achieved by exposing the naïve library to the peptides that form the antigenic region.

3.2. BLI-SELEX: Aptamer selection & characterization

The initial step of target loading is of prime-most importance, which determines the efficiency of the selection step. In supporting information ST9, Fig. S5 shows the normalized sensogram showing the gradual rise in response (Step 3) during the loading of target peptide onto the AR2G sensor, which causes an increase in biolayer thickness on sensor surface denotes immobilization of the peptide. Similarly, the rest of the peptides were loaded on respective sensors for the ensuing aptamer selection step.

These peptide coated sensors were then exposed to the naïve library, and the binders then dissociated gradually according to their binding strength. As illustrated in Fig. S1, the naïve library consisting of a random pool of oligomers interacts and binds to the target molecules with varying affinities attributed by their structure and sequence. Multiple oligomers interact with the target (not exclusively unique sequence), which are sequentially dissociated from the target by dipping in individual wells containing dissociation buffers of increasing strength. The progression of SELEX was monitored in real-time, and Fig. 2a shows the sensogram of an association-dissociation cycle of peptide stx1.1 coated AR2G sensor. The steep increase in binding response in association step shows the fishing of sequences from exposed oligomer library and subsequent dips are recorded sequentially after the oligo/peptide complex is allowed to dissociate in increasing concentration of NaCl (0.1–1 M), depicting a decrease in the biolayer formed on the sensor and henceforth shedding of sequences from the peptide coated sensor. Besides, for the enrichment of other possible aptamers from the naïve library, the process was repeated multiple times (Fig. 2b). However, it was observed that in the first association itself most of the binders from the library had interacted with the sensor, and an almost negligible association was recorded in further iterations (inset in Fig. 2b). This efficiency can be attributed to the interacting potency of the various sequences of the naïve library with the chosen target and will tend to differ with different library-target combinations. In our present study, noteworthy results were obtained with the single primary cycle, and further enrichment did not significantly enhance the screening process, as evident from Fig. 2b. From the first round (Fig. 2c), the initial two elutes (0.1–0.2 M) were disregarded due to the nominal stringency of their dissociation buffer, which merely constituted as wash buffers. Thus, the latter DNA elutes pools in higher strength buffers were chosen, purified, amplified, and studied for binding affinity against the target peptide. These dissociated molecules (13.9 ng μL^{-1}) collectively constituted ~56% sequences of the exposed naïve library (24.5 ng μL^{-1}). In our knowledge, such binding efficiency from a single initial SELEX cycle has not been reported yet and particularly for the first time using BLI SELEX. Furthermore, the binding sensogram in Fig. 2d shows the massive difference in the association curve of the eluted pools, denoting an increase in binding affinity of latter fractions. The pool with the best binding

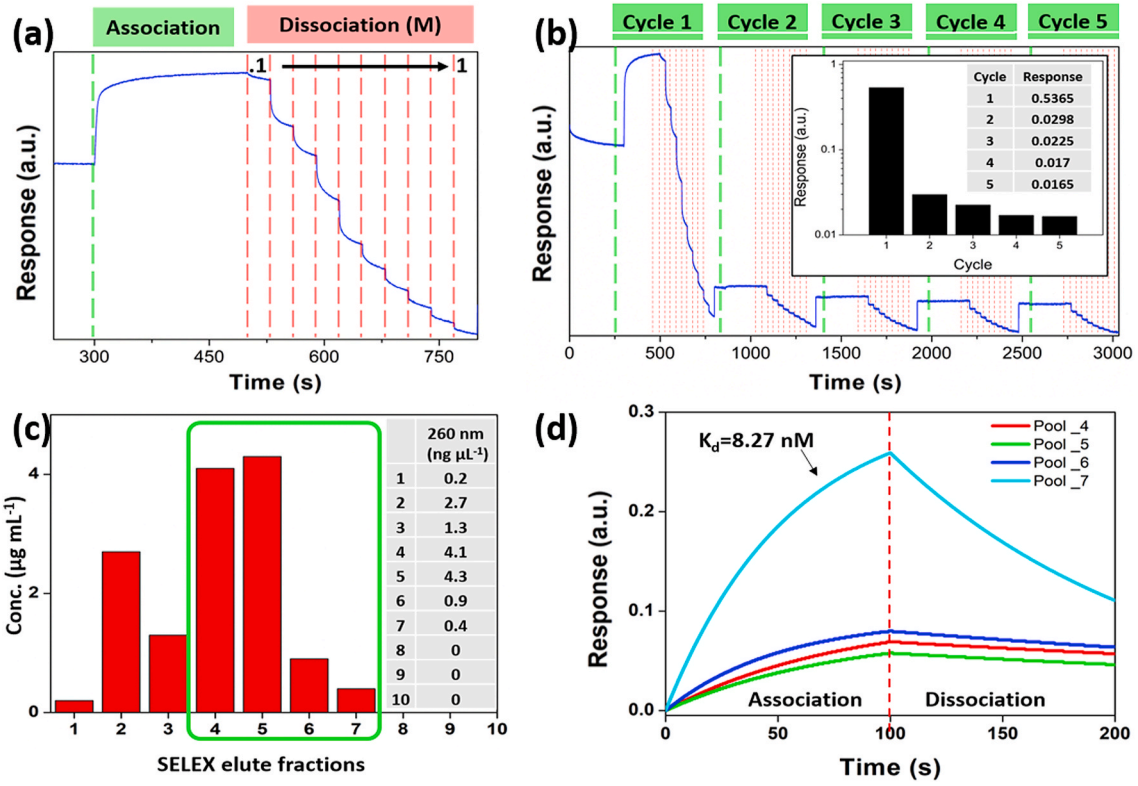

Fig. 2. BLI-SELEX for stx1.1. A high-throughput facile selection method for aptamer selection against epitopic peptide stx1.1. (a) Sensogram of a cycle showing association-dissociation kinetics of stx1.1 coated AR2G sensor with oligomer library & subsequent dissociation with increasing concentration of NaCl (0.1–1 M). (b) SELEX cycle iterations to enrich binders from the naïve library and the binding response to target with each iteration shown as a histogram (*inset*). The elutes at each step were collected, amplified, and analyzed for the presence of binders. (c) Spectrophotometric quantification ($\lambda_{260\ nm}$) of ssDNA in elutes. The highlighted elutes were purified, amplified & generated aptamer pools characterized for binding affinity. (d) Sensogram is showing the association-dissociation curves of selected positive pools & aptamer pool 7 with best K_d = 8.27 nM against peptide stx1.1 was chosen for further binding interaction with the toxin, stx1b.

affinity (in this particular case) pool 7 with $K_d = 8.27$ nM against peptide stx1.1 was chosen for further study. Conclusively, similar studies were carried out for other epitopes of stx1 & stx2 (Supporting Information ST10; Fig. S6 & ST11; Figs. S7–9) and the best-of-pool aptamer selected. The selected pools were cloned and sequenced, providing multiple aptamer sequences, out of which few were chosen based on their variability in cladogram phylogenetic tree clusters (Supporting Information ST12; Fig. S10) generated by Clustal Omega online tool (https://www.ebi.ac.uk/Tools/msa/clustalo/) and G-quadruplex propensity were used for further application. The binding affinity of the selected aptamers with the whole protein toxin was analyzed using BLI at various concentrations of the individual champion aptamers for stx1 and stx2. The average K_d values were determined using 1:1 global fitting of target vs. ligand and the mean value estimated from the different concentrations, as shown in Fig. S11 (Supporting Information ST13). The representative sensograms at 100 nM aptamer concentration for the selected aptamers against stx1 and stx2 have been shown in Fig. 3a and b, respectively, and the dissociation constants of various aptamers along with their sequences in Fig. 3c. It was observed that Apt(Stx1.1) and Apt (Stx2.3) showed low dissociation constants of 47.2 pM and 28.6 pM, respectively, with their cognate toxins. These binding capabilities of the selected champion aptamers were further corroborated using fluorescence plate binding assay (Supporting Information ST14; Fig. S12), showing kinetics with a good coefficient of determination value $R^2 > 0.9$.

A manifold increase in binding affinity from apta-peptide interaction to apta-toxin interaction was observed, which may be attributed to two prominent phenomena; (i) the increase in binding sites resulting in higher avidity and; (ii) facilitated binding of subsequent aptamer molecules to the target. Out of the clones sequenced, those conforming to Guanine-quadruplex (G-quad) motifs in sequence regions were analyzed, therein Apt(Stx1.1) containing G-quad from N^{29}–N^{53} and N^{62}–N^{76} & in Apt(Stx2.3) from N^{19}–N^{45} were successfully selected (Fig. 4). The mfold tool generated putative structures of the selected aptamers presented in Fig. S13 (Supporting Information ST15) show different structural conformations and thermodynamic properties of the sequences Apt(Stx1.1) and Apt(Stx2.3) at standardized binding buffer ionic conditions of $[Na^+] = 0.10$ M, $[Mg^{2+}] = 0.005$ M at 37 °C. The individual structures with the lowest ΔG (-3.29 kcal mol^{-1} and -5.67 kcal mol^{-1}) for the two subtypes were chosen, and their structure models rendered. Both of these aptamers as seen in Fig. 4 showed significant secondary structural elements viz., stacks, helix & loops resulting in high complexity structures with Apt(Stx1.1) showing a hairpin loop motif from G^{48} – T^{54} and Apt(Stx2.3) showing three prominent hairpin loops viz., G^{65}-C^{70}, C^{41}-G^{55}, and G^{13}-C^{27}. These putative structures were also generated for the selected aptamers at varying $[Na^+] = 0.1$–1 M, showing that the secondary structure of the aptamer (Supporting Information ST15, S14). Though rigid within some concentration range, the aptamers changed their folded conformation when the environmental salt concentration was considerably altered. Given this, though the oligomer structures would vary in different dissociating buffers during the BLI-SELEX, for the study of association interaction and as well in further application studies, the concentration of Na^+ was kept standard at 0.1 M in the binding buffer. Thus, for all our other simulations, this parameter has been fixed for the ease of our experimental study. The docking studies simulated for apta-peptide interactions were carried out using Zdock (version 3.0.2) at an interparticle distance of 1.2 Å in the vacuum, which showed extensive intramolecular polar interactions & conformational fitting of the target into the aptamer binding pockets (Fig. 4). Though this interaction might vary in the solution phase, this is a preliminary attempt in understanding bio-interaction amongst the target and ligand. These well-characterized champion aptamers (with the highest K_d value to protein toxin) were chosen as bio-receptors for subsequent bio-sensing assays.

3.3. Synthesis & characterization of Chito-WSe_2 nanosensor

The results detailing the characterization of the nanostructure is shown in Supporting Information ST16; Fig. S15. The liquid exfoliated Chito-WSe_2 nanosheets appeared as a reddish dispersion (inset of Fig. S15a). It can be easily observed that with increasing concentration of chitosan, the extent of exfoliation increased as depicted in Fig. S15a. Higher concentrations were observed to have increased viscosity, difficult for homogenous dilutions & correct estimations. A good exfoliated

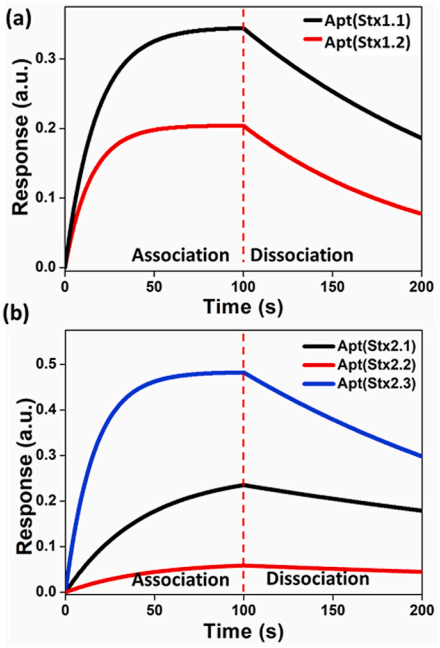

(c)

Peptide	Aptamer	K_d (peptide)	K_d (protein)
Stx1.1	Apt(Stx1.1) ATCCAGAGTGACGCAGCAGTAGTTTGTT GGTTATTACGGCGGGTTGCGATGGGTGC GAATCGGTGGACACGGTGGCTTAGT	8.27 nM	47.2 pM
Stx1.2	Apt(Stx1.3) ATCCAGAGTGACGCAGCAGGATAGGAC GTCAAATTAGGGCCCGGTACAACGAAA GCCCACAACTGGACACGGTGGCTTAGT	31.0 nM	30.3 μM
Stx2.1	Apt(Stx2.1) ATCCAGAGTGACGCAGCAGGGGGCAGG TTCATGGCTTGGGTGCGGTGGGCATGAT TCGTGGTGTGGACACGGTGGCTTAGT	45.2 nM	83.8 nM
Stx2.2	Apt(Stx2.2) ATCCAGAGTGACGCAGCATGTATCTCTTA CTTAAGCCTTTGGTTCGGTAACAGCCTG GCATGCTGGACACGGTGGCTTAGT	110 nM	25.2 μM
Stx2.3	Apt(Stx2.3) ATCCAGAGTGACGCAGCAGGAAAGGAC GTCAAATTAGGGGCCGGGACAACGAAA GCCCACAACTGGACACGGTGGCTTAGT	4.6 nM	28.6 pM

Fig. 3. Binding affinity results. BLI binding affinity assays for best-of-pool aptamers at 100 nM concentration against whole protein toxin (a) stx1 & (b) stx2 showing functional association-dissociation kinetics. (c) List of best-of-pool aptamers along with their average K_d values against both targeted epitope peptides & whole cognate toxins.

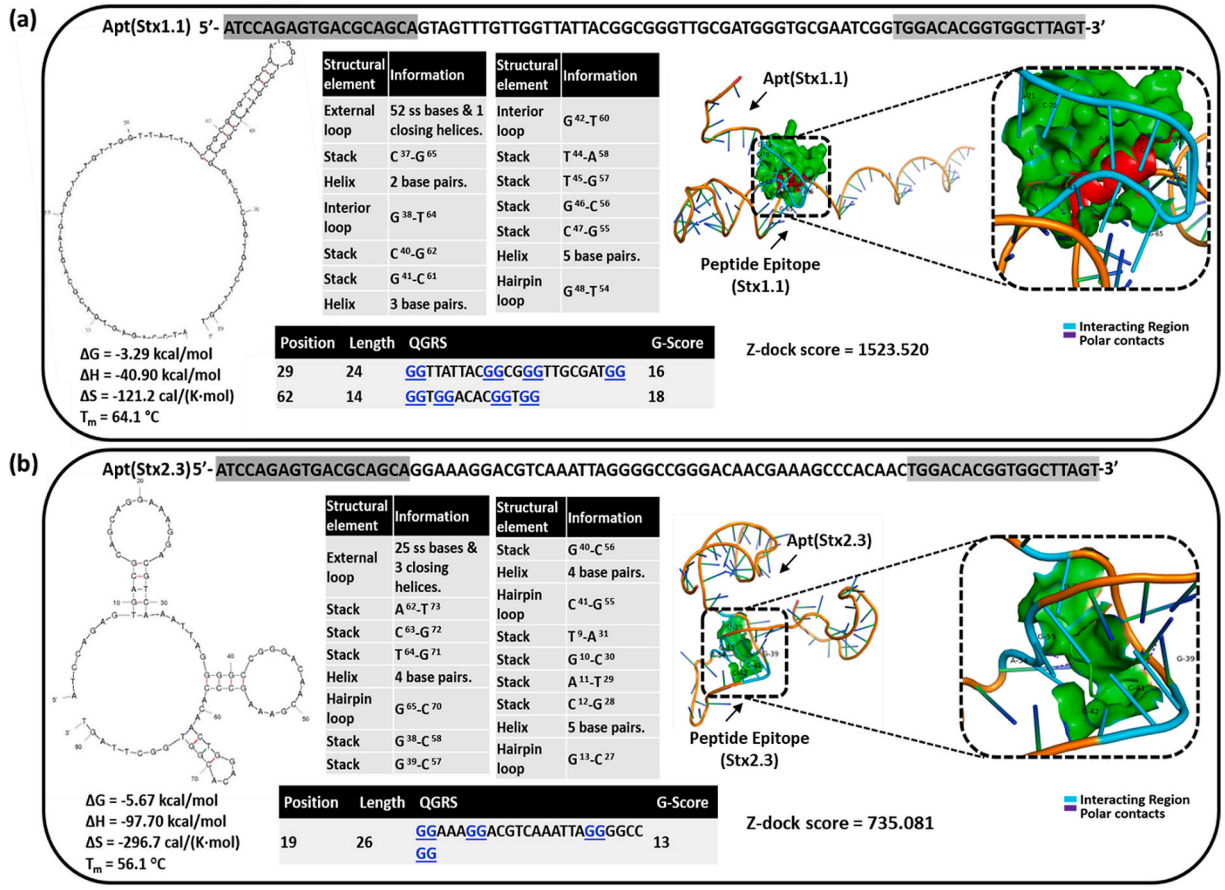

Fig. 4. Structure and docking studies. The Mfold structures (*left*) of selected aptamers (a) Apt(Stx1.1) and (b) Apt(Stx2.3) were found to have G-quadruplex estimated by using Quadruplex forming G-rich Sequences (QGRS) online tool. Out of the several possibilities, the structures with the lowest Gibbs free energy were selected, and their 3D model rendered. The aptamers showed significant elements viz., stacks, helix, and loops resulting in high complexity structures (shown in tabular format). The Zdock studies (*right*) were simulated for apta-peptide showing both intramolecular polar interactions and structural fitting of binding pockets. The cyan highlighted region depicts the interacting region of the DNA aptamer with the respective target peptide. (For interpretation of the references to colour in this figure legend, the reader is referred to the Web version of this article.)

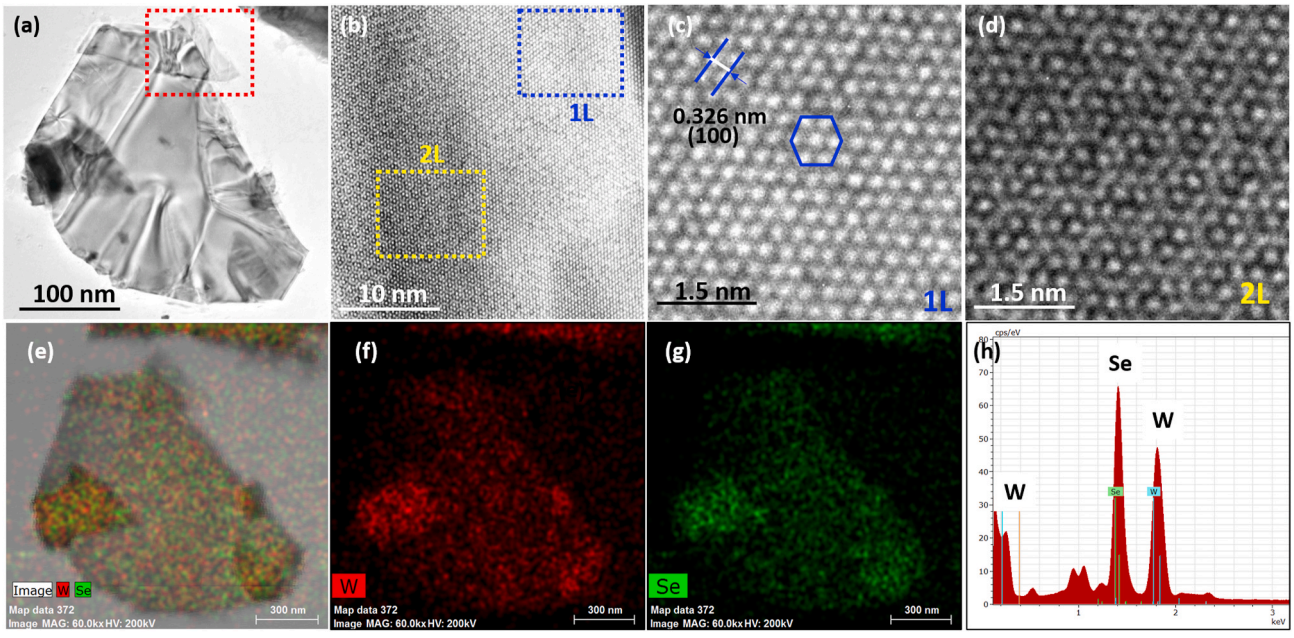

Fig. 5. TEM micrographs. Displaying low magnification image of (a) exfoliated chito-WSe_2 nanosheet (b) magnified few-layer region of overlapped flakes & high-resolution images of (c) monolayer & (d) bilayer region along with (e-g) corresponding EDX elemental mapping & spectra.

nanomaterial amount (0.43 mg exfoliated per 1 mg bulk) was obtained and used for further experiments. In the extinction spectra, typical excitonic peaks A & B corresponding to valence band split & spin-orbital coupling were well observed (Packiaseeli et al., 2016). As observed in Figs. S15b–c, the XRD spectra of bulk & exfoliated nanomaterial were consistent with the hexagonal lattice structure of WSe_2 (reference JCPDS card no. 00-038-1388), and a broad overlapped peak at 245 cm^{-1} for E^1_{2g} (in-plane) & A_{1g} (out-of-plane) were observed in Raman spectra. The reduction in peak intensity of (002) plane in XRD spectra and B^1_{2g} peak at 301 cm^{-1} in Raman spectra of exfoliated nanomaterial are indicative of few-layered sheets (Jia et al., 2017). AFM analysis revealed the ultrathin sheet-like nature of the Chito-WSe_2 of a thickness ~3 nm suggesting few-layered nanostructure (provided being chitosan-coated) with a lateral length of ~250 nm which was supported by TEM images (Figs. S15d–e). Additional HR-TEM images supplemented with EDX maps (Fig. 5) show the wrinkled few-layer sheets with mono & bilayers being observed. The hexagonal symmetry of 2H–WSe_2 with a lattice spacing of 0.3 nm corresponding to a single layer (100) plane was seen (Wu et al., 2019).

3.4. Toxin detection: Aptamer mediated voltammetric assay

As detailed in Supporting Information ST17 for the efficient functionalization of aptamer onto the nanomaterial, pH-dependent zeta potential studies were carried out, and Fig. S16 shows, pH 7.0 was chosen as the best environment of the immobilization of DNA. In the supporting information ST18, Fig. S17 shows the electrochemical characterization of the nanosensor. CV measurements optimized the amount of Chito-WSe_2 deposited onto working electrode of SPE. Maximum current response was observed for 5 μg of nanomaterial, and this optimized concentration was used for further modifications (Fig. S17a). The nanostructured sensor showed a linear increase in the current intensity with the square root of the increasing scan rate (10 mV s^{-1} to 100 mV s^{-1}), indicating the diffusion control process (Fig. S17b). A small drop in current in CV scan & R_{ct} value in EIS were observed upon aptamer immobilization, which proves its deposition on sensor surface (Figs. S17c–d). The SEM studies of sensor surface showed good area coverage and morphological change of the sensor surface upon aptamer immobilization, validating efficient functionalization (Supporting Information ST19; Fig. S18).

The respective Apt(Stx1.1) & Apt(Stx2.3) modified nanosensors were used for the detection of respective toxin subtypes using the SWV technique. Fig. 6 shows a sequential decrease in current when the sensors were subjected to cognate toxin stx1, with a linear range of detection from 50 pg to 100 ng. The developed nanosensor showed a sensitivity of ~5 μA ng^{-1} mL with a LOD of 44.5 pg mL^{-1} for toxin stx1and 41.3 pg mL^{-1} for stx2 (Supporting Information ST20; Fig. S19). The selectivity of the sensors for target toxins far exceeded that of cross-reactive toxin subtype and other interfering proteins or polysaccharides (Fig. 6c). The application of the sensors for toxin detection in real spiked samples showed results comparable to control. A relatively more substantial drop in current was observed when 1% FBS was used, which can be attributed to high protein content. Nonetheless, both the sensors showed minimal cross-reactivity, a wide dynamic range of detection & low detection limit owing to the synergistic effect of picomolar affinity recognition moieties & conductive nature of exfoliated TMD. The superiority of this work can be easily validated from its comparison (Supporting Information ST21; Table S3) with other platforms reported for Shiga toxin detection.

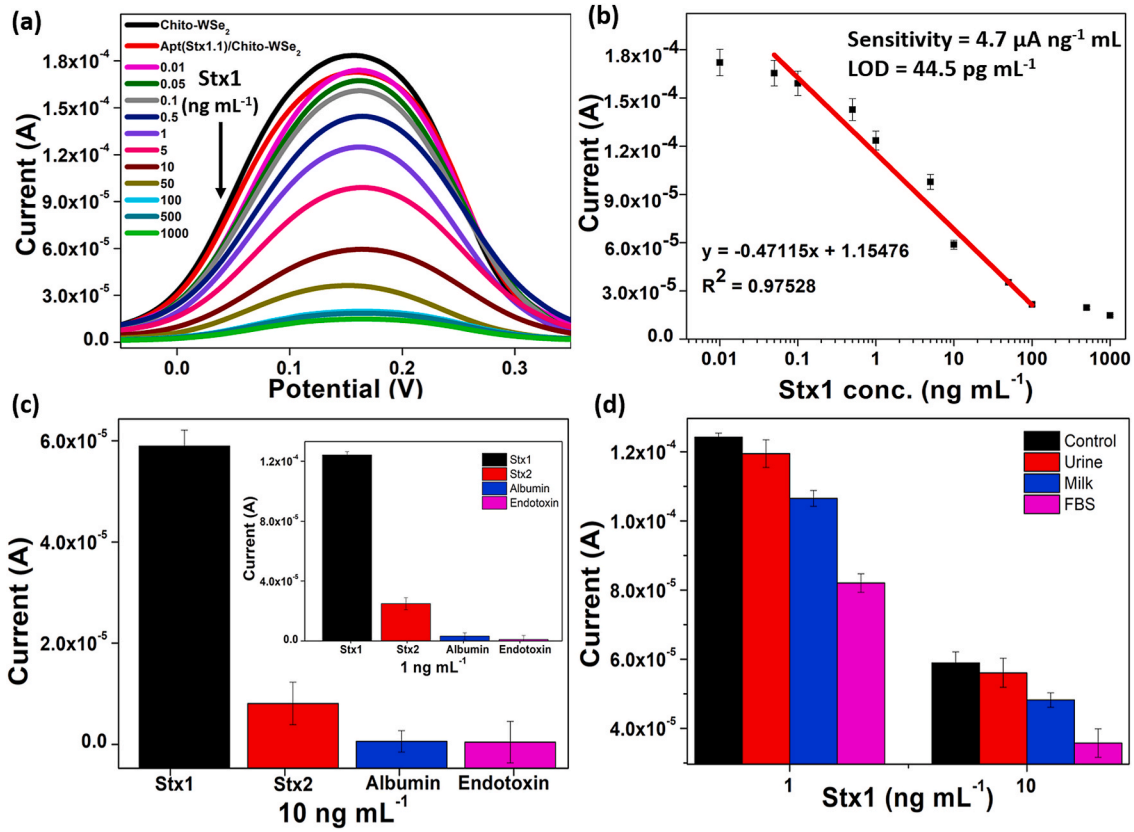

Fig. 6. Voltammetry bioassay for stx1. (a) SWV curves showing a reduction in peak current upon sensing of stx1 and (b) calibration curve showing linear response range. (c) Bar graph showing the comparative response upon detection of other cross-reactive molecules at 10 ng mL^{-1} and (inset) 1 ng mL^{-1} (d) bar graph depicting SWV response of developed aptasensor in pre-processed spiked real samples at both 1 & 10 ng mL^{-1}.

4. Conclusion

The study reports real-time & label-free aptamer selection using BLI-SELEX, yielding novel high-affinity aptamers against antigenically distinct *E. coli* Shiga toxins subtypes via specific epitopic peptides. These fully characterized aptamers, Apt(Stx1.1) & Apt(Stx2.3) with a pico-molar affinity of K_d (~47pM & ~29 pM, respectively) were successfully used to fabricate respective voltammetric diagnostic assays via immobilization onto chitosan exfoliated & functionalized 2D tungsten diselenide nanosheet platforms. These aptamers modified nanosensors showed high sensitivity of ~ 5.0 μA ng^{-1} mL, a dynamic response range from 50 pg mL^{-1} to 100 ng mL^{-1} with a detection limit of 44.5 pg mL^{-1} & 41.3 pg mL^{-1} for stx1 & stx2, respectively with low cross-reactivity in spiked urine, serum and milk samples.

CRediT authorship contribution statement

Harmanjit Kaur: Conceptualization, Formal analysis, Investigation, Writing - original draft, Writing - review & editing, Visualization. **Munish Shorie:** Methodology, Formal analysis, Writing - review & editing. **Priyanka Sabherwal:** Conceptualization, Resources, Writing - review & editing, Supervision.

Declaration of competing interest

The authors declare that they have no known competing financial interests or personal relationships that could have appeared to influence the work reported in this paper.

Acknowledgments

The authors acknowledge DST Nanomission Project (https://doi.org/10.13039/501100005052) (No. SR/NM/NS-1510/2014-G) for financial funding. HK and MS acknowledge INST-PhD and CSIR-JRF for fellowships. The authors acknowledge the technical support of Mrs. Baljeet Kaur, Mr. Sandeep, Mr. Pulkit Bindra & Ms. Mamta Raturi for TEM, SEM, XRD & AFM characterizations, respectively. The authors thank Dr. Sharmistha Sinha from INST, Mohali, for providing laboratory facilities & resources for experimental studies. The authors also thank Dr. Sharmistha Sinha from INST, Mohali, for providing laboratory facilities & resources for experimental studies.The authors also acknowledge the technical support of Mrs. Baljeet Kaur, Mr. Sandeep, Mr. Pulkit Bindra & Ms. Mamta Raturi for TEM, SEM, XRD & AFM characterizations, respectively.

Appendix A. Supplementary data

Supplementary data to this article can be found online at https://doi.org/10.1016/j.bios.2020.112498.

References

Challa, S., Tzipori, S., Sheoran, A., 2014. J. Nucleic Acids 2014, 1–8, 214929.
Chen, A., Shah, B., 2013. Anal. Methods 5 (9), 2158–2173.
Correia, B.E., Bates, J.T., Loomis, R.J., Baneyx, G., Carrico, C., Jardine, J.G., Rupert, P., Correnti, C., Kalyuzhniy, O., Vittal, V., Connell, M.J., Stevens, E., Schroeter, A., Chen, M., MacPherson, S., Serra, A.M., Adachi, Y., Holmes, M.A., Li, Y., Klevit, R.E., Graham, B.S., Wyatt, R.T., Baker, D., Strong, R.K., Crowe, J.E., Johnson, P.R., Schief, W.R., 2014. Nature 507, 201–206.
Dupont, D.M., Larsen, N., Jensen, J.K., Andreasen, P.A., Kjems, J., 2015. Nucleic Acids Res. 43.
Goto, S., Tsukakoshi, K., Ikebukuro, K., 2017. Biotechnol. Bioeng. 114 (12), 2706–2716.
He, X., Patfield, S., Hnasko, R., Rasooly, R., Mandrell, R.E., 2013. PLoS One 8.
Ikebukuro, K., Kiyohara, C., Sode, K., 2004. Anal. Lett. 37, 2901–2909.
Jia, X., Bai, J., Ma, Z., Jiang, X., 2017. J. Mater. Chem. B 5, 269–278.
Kaur, H., Garg, A., Raghava, G.P.S., 2007. Protein Pept. Lett. 14, 626–631.
Kaur, H., Shorie, M., Sabherwal, P., 2020. Microchim. Acta 187, 461.
Kaur, H., Shorie, M., Sharma, M., Ganguli, A.K., Sabherwal, P., 2017. Biosens. Bioelectron. 98, 486–493.
Kavaliauskiene, S., Dyvelingelem, A.B., Skotland, T., Sandvig, K., 2017. Toxins (Basel). 9, 44.
Kelly-Cirino, C.D., Nkengasong, J., Kettler, H., Tongio, I., Gay-Andrieu, F., Escadafal, C., Piot, P., Peeling, R.W., Gadde, R., Boehme, C., 2019. BMJ Glob. Heal. 4, e001179.
Kirk, M.D., Pires, S.M., Black, R.E., Caipo, M., Crump, J.A., Devleesschauwer, B., Döpfer, D., Fazil, A., Fischer-Walker, C.L., Hald, T., Hall, A.J., Keddy, K.H., Lake, R. J., Lanata, C.F., Torgerson, P.R., Havelaar, A.H., Angulo, F.J., 2015. PLoS Med. 12, e1001921.
Klausen, M.S., Jespersen, M.C., Nielsen, H., Jensen, K.K., Jurtz, V.I., Sønderby, C.K., Sommer, M.O.A., Winther, O., Nielsen, M., Petersen, B., Marcatili, P., 2019. Proteins Struct. Funct. Bioinformat. 87, 520–527.
Kozlova, E.E.G., Cerf, L., Schneider, F.S., Viart, B.T., NGuyen, C., Steiner, B.T., de Almeida Lima, S., Molina, F., Duarte, C.G., Felicori, L., Chávez-Olórtegui, C., Machado-de-Ávila, R.A., 2018. Sci. Rep. 8, 1–13.
Krieger, E., Koraimann, G., Vriend, G., 2002. Proteins Struct. Funct. Bioinformat. 47, 393–402.
Kudłak, B., Wieczerzak, M., 2020. Crit. Rev. Environ. Sci. Technol. 50, 816–867.
Kumar, V., Brent, J.R., Shorie, M., Kaur, H., Chadha, G., Thomas, A.G., Lewis, E.A., Rooney, A.P., Nguyen, L., Zhong, X.L., Burke, M.G., Haigh, S.J., Walton, A., McNaughter, P.D., Tedstone, A.A., Savjani, N., Muryn, C.A., O'Brien, P., Ganguli, A. K., Lewis, D.J., Sabherwal, P., 2016. ACS Appl. Mater. Interfaces 8, 22860–22868.
Li, F., Yu, Z., Han, X., Lai, R.Y., 2019. Anal. Chim. Acta 1051, 1–23.
Meirinho, S.G., Dias, L.G., Peres, A.M., Rodrigues, L.R., 2016. Biotechnol. Adv. 34 (5), 941–953.
Mejías, M.P., Hiriart, Y., Lauché, C., Fernández-Brando, R.J., Pardo, R., Bruballa, A., Ramos, M.V., Goldbaum, F.A., Palermo, M.S., Zylberman, V., 2016. Sci. Rep. 6, 24913.
Negahdary, M., 2020. Biosens. Bioelectron. 152, 112018.
Packiaseeli, S.A., Rajendran, V., Vijayalakshmi, R., 2016. Nanosyst. Phys., Chem. Math. 7, 703–706.
Panigaj, M., Johnson, M.B., Ke, W., McMillan, J., Goncharova, E.A., Chandler, M., Afonin, K.A., 2019. ACS Nano 13 (11), 12301–12321.
Pehlivan, Z.S., Torabfam, M., Kurt, H., Ow-Yang, C., Hildebrandt, N., Yüce, M., 2019. Microchim. Acta 186 (8), 563.
Rahman, M., Nabi, A., Asadulghani, M., Faruque, S.M., Islam, M.A., 2018. BMC Microbiol. 18, 98.
Rahmanian, E., Mayorga-Martinez, C.C., Malekfar, R., Luxa, J., Sofer, Z., Pumera, M., 2018. ACS Appl. Nano Mater. 1, 7006–7015.
Sharifi, S., Vahed, S.Z., Ahmadian, E., Dizaj, S.M., Eftekhari, A., Khalilov, R., Ahmadi, M., Hamidi-Asl, E., Labib, M., 2020. Biosens. Bioelectron. 150, 111933.
Shi, Q., Shih, E.-M., Gustafsson, M.V., Rhodes, D.A., Kim, B., Watanabe, K., Taniguchi, T., Papić, Z., Hone, J., Dean, C.R., 2020. Nat. Nanotechnol. 15, 569–573.
Shorie, M., Kumar, V., Kaur, H., Singh, K., Tomer, V.K., Sabherwal, P., 2018. Microchim. Acta 185.
Tuerk, C., Gold, L., 1990. Science 249, 505–510.
Uysal Unalan, I., Wan, C., Trabattoni, S., Piergiovanni, L., Farris, S., 2015. RSC Adv. 5, 26482–26490.
Vallières, E., Saint-Jean, M., Rallu, F., 2013. J. Clin. Microbiol. 51, 481–486.
Villalonga, A., Pérez-Calabuig, A.M., Villalonga, R., 2020. Anal. Bioanal. Chem. 412, 55–72.
Wang, T., Chen, C., Larcher, L.M., Barrero, R.A., Veedu, R.N., 2019. Biotechnol. Adv. 37, 28–50.
Wu, P.C., Yang, C.L., Du, Y., Lai, C.H., 2019. Sci. Rep. 9, 1–10.